AC and DC Conductivity in Nano- and Microcrystalline $Li_2O : B_2O_3$ Composites: Experimental Results and Theoretical Models

By Sylvio Indris[1], Paul Heitjans[1,*], Markus Ulrich[2], and Armin Bunde[2,*]

[1] Institut für Physikalische Chemie und Elektrochemie, Universität Hannover, Callinstraße 3–3a, 30167 Hannover, Germany
[2] Institut für Theoretische Physik III, Justus-Liebig-Universität Gießen, Heinrich-Buff-Ring 16, 35392 Gießen, Germany

Dedicated to Prof. Dr. Klaus Funke on the occasion of his 60th birthday

We report on impedance measurements of nano- and microcrystalline composites of the Li ion conductor Li_2O and the ionic insulator B_2O_3 as well as their interpretation in the frame of percolation models. In the experimental part, besides the dc conductivity and its dependence on composition and temperature (*i.e.* its activation energy) also the ac conductivity and its dependence on composition, temperature and frequency (*i.e.* the conductivity exponent) are presented. Striking differences between the nanocrystalline and the corresponding microcrystalline composites were found. Deviations of the ac from the dc results can be explained by the fact that the experiments probe ion dynamics on different time and thus length scales. In the theoretical part, a continuum percolation model, a brick-layer type bond percolation approach and a Voronoi construction are alternatively used to model the dc behaviour. Based merely on the largely different volume fractions of the interfaces between ionic conductor and insulator grains in the nano- and microcrystalline composites, good overall agreement with the experimental dc results is obtained. The high critical insulator content above which the experimental conductivity vanishes in the nanocrystalline composites suggests the presence of an additional Li diffusion passageway of nanometer length in the interface between nanocrystalline insulator grains.

---

* Corresponding authors.
E-mail: heitjans@pci.uni-hannover.de; Armin.Bunde@physik.uni-giessen.de

1. Introduction

Nanocrystalline materials are compacted, polycrystalline materials with crystallite sizes in the range of typically 5 to 50 nm [1–3]. They often show enhanced diffusivity when compared to their coarse grained counterparts [4–6]. In ionic materials, the enhanced diffusivity leads to an increased ionic conductivity which is attractive with respect to possible applications in battery systems, fuel cells or sensors. Here we are interested in nanocrystalline composite materials, where in addition to the interfaces between like grains interfaces between unlike grains exist, which can lead to the formation of ionic space charge layers and thus to an even more enhanced conductivity [7–10]. Besides the variation of the grain size the changing of the composition of such materials offers an additional degree of freedom to tailor the macroscopic properties of these composites. This was shown for the dc conductivity of nanocrystalline $(1-x)\mathrm{Li_2O} : x\mathrm{B_2O_3}$ composites where (except for x close to one) the increased conductivity of the interfaces between unlike $\mathrm{Li_2O}$ and $\mathrm{B_2O_3}$ grains leads to an enhancement of the overall dc conductivity by a factor of about 10 compared to pure $\mathrm{Li_2O}$ [11]. In this paper we compare the dc and ac conductivity of such composites to get more insight into the short-range motion of the Li ions and to elucidate the influence of the morphology of the network of fast diffusion pathways formed by the different interfaces in these samples. Furthermore, we present various theoretical approaches, by which the dependence of the dc conductivity on the composition of these materials can be described, and discuss the advantages and disadvantages of these models.

2. Sample preparation and experimental setup

The nanocrystalline oxides $\mathrm{Li_2O}$ and $\mathrm{B_2O_3}$ were prepared by high-energy ball milling from the coarse grained source materials [12, 13]. All preparation steps were done in dry argon atmosphere to prevent contact of the samples with water or CO_2. The air tight sample holder for the conductivity measurements was loaded with the sample and sealed in a glove box filled with dry argon. X-ray diffraction and transmission electron microscopic measurements show that milling for 8 h is sufficient to reduce the grain size down to about 20 nm. Differential thermal analysis showed that the nanocrystalline materials are stable at temperatures up to about 500 K. At higher temperatures grain growth sets in. For comparison we also prepared the microcrystalline counterparts from the unmilled source materials. The composites were prepared by mixing the appropriate amounts of the two components and compacted under uniaxial pressure of 1 GPa. Contacts for conductivity measurements were pressed from platinum powder to the pellets with the same pressure. The cylindrical samples had a diameter of 8 mm and a thickness of typically 1 mm. The ac conductivity of the composites was measured with a HP 4192 impedance analyzer in
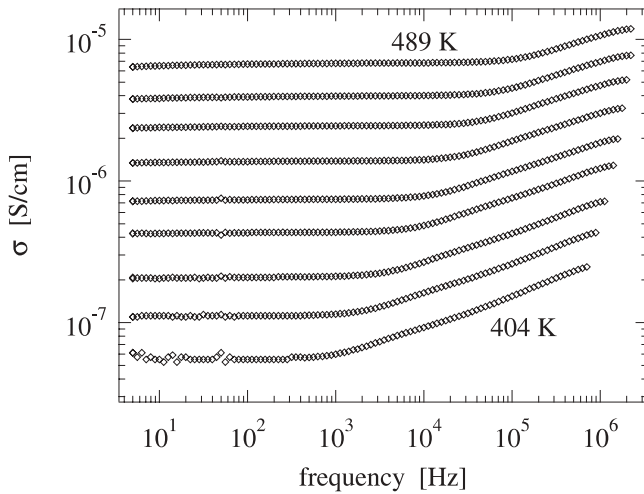
Fig. 1. Real part of the conductivity *vs.* frequency for nanocrystalline $(1-x)$Li$_2$O : xB$_2$O$_3$ for $x = 0.6$. The corresponding temperatures are 489 K, 478 K, 468 K, 457 K, 446 K, 436 K, 425 K, 414 K and 404 K (top to bottom).

the frequency range from 5 Hz to 13 MHz at temperatures between 300 K and 500 K.

3. Experimental results

Fig. 1 shows the real part of the conductivity of nanocrystalline $(1-x)$Li$_2$O : xB$_2$O$_3$ for $x = 0.6$ in the frequency range from 5 Hz to 1 MHz for temperatures between 404 K and 489 K. The characteristic features of these spectra which are common to all samples are *(i)* a plateau at low frequencies which reflects the dc conductivity of the samples and *(ii)* a dispersive region at high frequencies where the conductivity can be roughly described by a power law

$$\sigma(\omega) \propto \omega^n \tag{1}$$

with $0 < n < 1$. Both regions are separated by a cross-over regime. This overall behaviour has been found for many ionic conductors and is discussed in detail in, *e.g.*, [14–19]. In the following we study how the dc conductivity σ_{dc} (extracted from the low-frequency plateau) and the ac conductivity σ_{ac} (extracted at a frequency $\nu = \omega/2\pi = 100$ kHz) depend on the composition. Isotherms for 433 K are displayed in Fig. 2, where σ_{dc} and σ_{ac} are plotted as a function of both insulator mole content x and insulator volume fraction p; p and x are related by $p = \alpha x/(1 - x + \alpha x)$ where α is the ratio of the mole volumes of the insulator and the ionic conductor (about 1.91 here). For each composition, the measurements were done on two independently prepared samples. For comparison, we
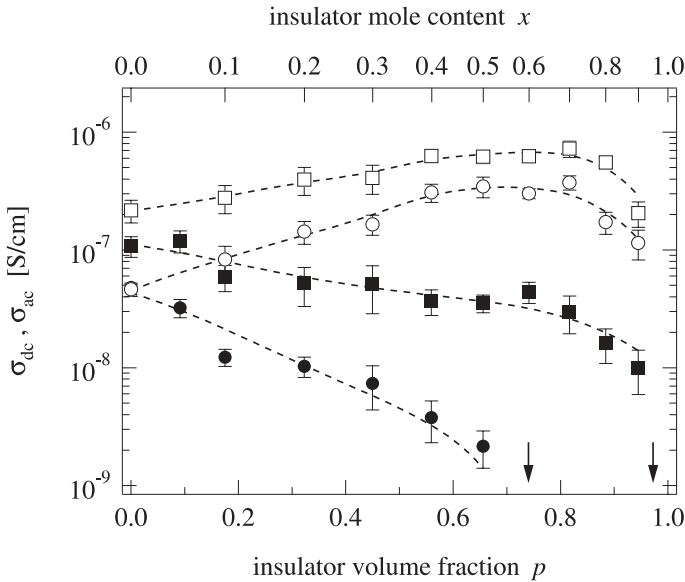
insulator mole content x

Fig. 2. Dc (circles) and ac (squares) conductivities of microcrystalline (full symbols) and nanocrystalline (open symbols) $(1-x)Li_2O : xB_2O_3$ composites *vs.* insulator volume fraction at 433 K. Dashed lines are drawn to guide the eye. The arrows indicate the compositions where the dc conductivity of the micro- and nanocrystalline materials show a sharp drop and fall below the detection limit.

also performed measurements on the corresponding microcrystalline samples. The data points in the graphs show the weighted average with weighted error bars. The dashed lines are guides to the eye.

Let us first concentrate on the dc conductivity. For pure Li_2O, *i.e.* $x = p = 0$, the dc conductivity of the microcrystalline and the nanocrystalline samples coincide. When Li_2O is successively substituted by B_2O_3, the two systems behave very different. In the microcrystalline samples, the dc conductivity decreases monotonically with x, while in the nanocrystalline samples, the dc conductivity first increases and reaches a maximum at $x \approx 0.6$ where the conductivity is about one order of magnitude larger than that of pure Li_2O. Further increase of the insulator content leads to a decrease of the conductivity. At $x = 0.95$, finally, the conductivity has dropped below the detection limit. We have shown before [11, 20], that the overall behaviour (including the differences between nano- and microcrystalline samples) can be explained by the assumption of an enhanced conductivity at the interfaces between unlike grains. Even more remarkable than the increase of the dc conductivity with increasing insulator content is the fact that, starting from the pure insulator B_2O_3, only a tiny volume fraction of Li_2O is needed to obtain a dc conductivity which is considerably higher than the dc conductivity of pure Li_2O.

Next we consider the ac conductivity σ_{ac}, which is represented by the squares in Fig. 2. For the nanocrystalline samples, σ_{ac} shows roughly the same behavior as σ_{dc}, but the increase of σ_{dc} at small insulator content is more pronounced than the increase of σ_{ac}. Of course, σ_{ac} is always above σ_{dc}. For the microcrystalline samples, in contrast, both quantities behave very different. While σ_{dc} decreases monotonically, falling below the detection limit above $x = 0.5$ resp. $p = 0.65$, σ_{ac} diminishes only slightly between $x = 0$ and $x = 0.1$. Between $x = 0.1$ and $x = 0.7$, σ_{ac} is roughly constant, and decreases slightly for x approaching 1.

The different behavior of σ_{ac} and σ_{dc} in the microcrystalline system can be understood by percolation theory [21]. The dc conductivity is a result of the long-range motion of the ions, which can take place only when a percolating conductive cluster exists. Hence, σ_{dc} is zero when, above the percolation threshold, this cluster no longer exists. On the other hand, σ_{ac} probes the ionic motion on shorter length scales, and thus is not connected with the existence of a percolating conductive cluster. As a result, σ_{ac} depends only slightly on the composition and shows a remarkable decrease only at very large insulator contents.

Next we discuss the behavior of the activation energies E_A, which describe the temperature dependence of σ_{ac} and σ_{dc}. In general, the activation energy is related to the conductivity by the Arrhenius relation

$$\sigma T = A \exp\left(-\frac{E_A}{k_B T}\right) , \tag{2}$$

where A is the pre-exponential factor, k_B the Boltzmann constant and T the temperature. Fig. 3 shows E_A, for both the dc and ac conductivities of both micro- and nanocrystalline samples, as a function of the insulator content. Again, the data points represent the average of two samples with equal compositions. For both the dc and ac conductivity, the activation energies of the nanocrystalline samples show only a weak dependence on the insulator content, with $E_{A,dc}^{nano} \approx 1\,eV$ for the dc conductivity and $E_{A,ac}^{nano} = 0.6\ldots 0.7\,eV$ for the ac conductivity. This is in contrast with the behaviour of the microcrystalline samples where the activation energy of σ_{dc} increases from $E_{A,dc}^{micro} \approx 0.9\,eV$ at $x = 0$ to $E_{A,dc}^{micro} \approx 1.2\,eV$ at $x = 0.5$ and the activation energy of σ_{ac} decreases from $E_{A,ac}^{micro} \approx 0.75\,eV$ at $x = 0$ to $E_{A,dc}^{micro} \approx 0.4\,eV$ at $x \approx 0.95$. The fact that in all cases the activation energy of the ac conductivity is lower than that of the dc conductivity again reflects that the ac conductivity probes dynamics on shorter time and thus length scales.

Fig. 4 finally shows the effective conductivity exponent n (see Eq. (1)) of the micro- and nanocrystalline samples, extracted from the dispersive region, as a function of the insulator content x. In the microcrystalline samples, n increases with x, i.e. the dispersion becomes stronger with x. This reflects the behavior seen in Fig. 2 where the difference between the ac and the dc conduc-
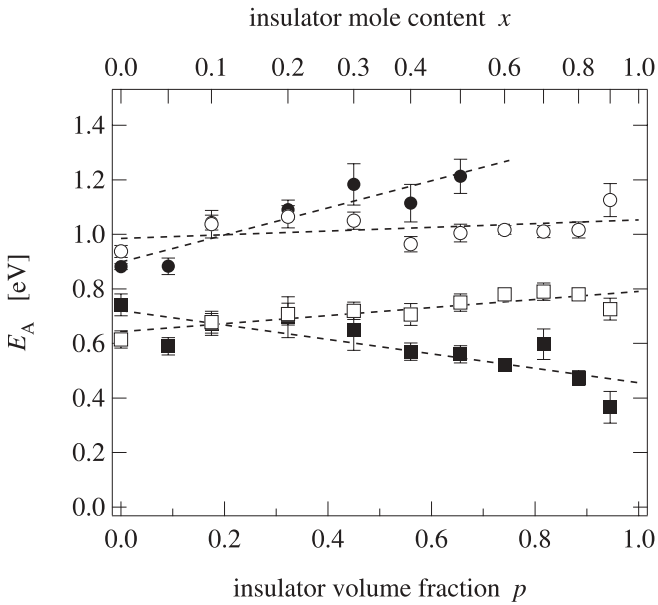
insulator mole content x

Fig. 3. Activation energies of the dc (circles) and ac (squares) conductivity of microcrystalline (full symbols) and nanocrystalline (open symbols) $(1-x)\mathrm{Li_2O} : x\mathrm{B_2O_3}$ composites *vs.* insulator volume fraction.
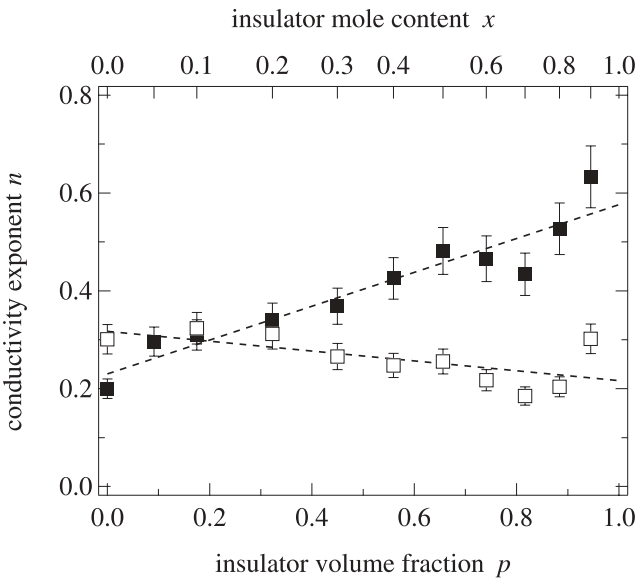
insulator mole content x

Fig. 4. Exponent n (*cf.* Eq. (1)) for the ac conductivity of microcrystalline (■) and nanocrystalline (□) $(1-x)\mathrm{Li_2O} : x\mathrm{B_2O_3}$ composites *vs.* insulator volume fraction.
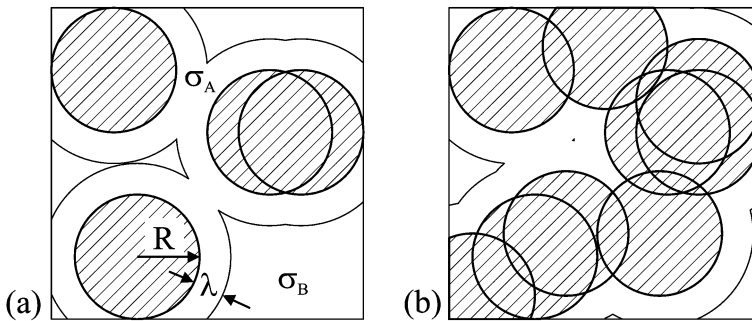
Fig. 5. Continuum percolation model with insulating spheres (radius R) dispersed in an ionic conductor (conductivity σ_B) and a highly conducting interface (conductivity σ_A, thickness λ), after [23]. The figures show the two critical insulator contents where (a) infinite highly conducting pathways are formed and (b) these pathways are disrupted.

tivity increases with x. In the nanocrystalline samples, in contrast, n decreases slightly with x again in accordance with Fig. 2 where the difference between ac and dc conductivity decreases with x.

4. Models

4.1 Continuum percolation model

The increase of the ionic conductivity at intermediate insulator contents for the nanocrystalline composites clearly shows that the interfaces between the two components are responsible for the conductivity enhancement. To describe the dependence of the dc conductivity of the composites on the insulator content p, we first employed a continuum percolation model [22, 23] which is sketched in Fig. 5. The insulating particles are represented by spheres with radius R. Around these insulating particles a highly conducting interface with width λ and ionic conductivity σ_A is created. The remaining volume represents the ionically conducting phase which has a conductivity σ_B. We consider an enhancement factor $\tau = \sigma_A/\sigma_B$ of 100 and an interface thickness $\lambda = 1\,nm$. The grain radii R have been determined by transmission electron microscopy and X-ray diffraction [12, 13] and are roughly $5\,\mu m$ for the microcrystalline composites and $10\,nm$ for the nanocrystalline composites. The overall conductivity of the system was then calculated by an effective medium approximation [11]. The results are shown in Fig. 6, where they are also compared with the experimental results for the dc conductivity. A good overall agreement is found. However, the effective coordination numbers z used in this approach as fit parameters to reproduce the experimental results ($z = 7$ for the microsystem and $z = 59$ for the nanosystem) can hardly be rationalized.
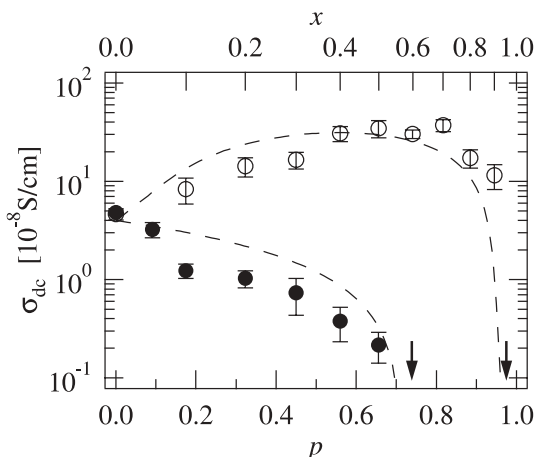
Fig. 6. Results of the continuum percolation approach (dashed lines) compared to the experimental results for the dc conductivity at 433 K, after [11]. The arrows indicate the compositions where the dc conductivities fall below the detection limit.

4.2 Brick-layer type percolation model

In an attempt to understand the experimental results on a more microscopic basis, we have considered a brick-layer type model where both, micro- and nanocrystalline composites are treated on the same footing [20]. In the model, we start with a cubic box of size L^3 that is divided into a large number of small cubes with equal volumes a^3. Each of the small cubes is regarded as a grain of the composite. With a given probability p the cubes are supposed to be insulating B_2O_3 grains. Thus the volume fraction of the Li_2O grains is $1-p$. By definition, conducting grains are connected when they have one corner in common. Fig. 7(a) shows the largest cluster of Li_2O grains that connects opposite faces of the large box close to the percolation threshold, at $p = 0.9$. Again we assume a highly conducting interface of width λ between insulating and ionically conducting particles. Next we replace the small cubes in Fig 7(a), that represent the Li_2O grains, by a bond lattice sketched in Fig. 7(b). The bonds represent the ionic conduction *(i)* inside the grain (Σ_0), *(ii)* along the interface area (Σ_1) and *(iii)* along the interface edges (Σ_2). The length of each bond is $a/2$. The cross section each bond represents is $(a-\lambda)^2$ for the Σ_0 bonds, $(a-\lambda)\lambda$ for the Σ_1 bonds and λ^2 for the Σ_2 bonds. Having this in mind, the conductance of each bond can be calculated easily. We assume that *(i)* in the bulk of the insulating B_2O_3 grains, the specific conductivity is zero, that *(ii)* in the bulk of the conducting Li_2O grains as well as in the interfaces between them, the specific conductivity is σ_B, and that *(iii)* Li_2O grains in contact with a B_2O_3 grain share a highly conducting interface with specific conduc-
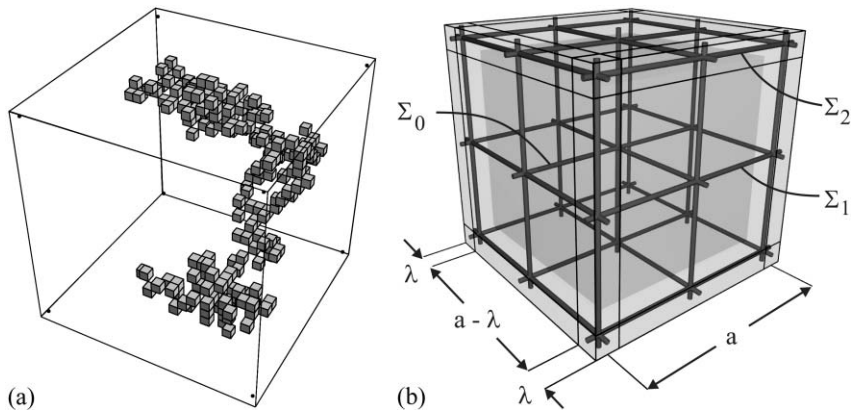
Fig. 7. (a) The largest cluster of insulating particles for the brick-layer type model in three dimensions at the critical concentration. (b) A single grain and the bonds assigned to conduction in the interior of the grains, along the sides and along the edges of the grain [20].

tivity $\sigma_A = \tau\sigma_B$. The enhancement factor τ is assumed to be of the order of $10^2 - 10^3$.

Finally, for calculating the total conductivity of the composite we map the problem onto the corresponding diffusion problem by defining appropriate jump rates (proportional to the bond conductances) along the bonds. For given values of τ, a, λ and p, we then determine the mean square displacement $\langle r^2(t)\rangle$ of many random walks as a function of time t on the largest cluster of each model system, average over all of them, and obtain the diffusion coefficient $D = \lim_{t \to \infty}\langle r^2(t)\rangle/6t$, which is related to the dc conductivity by the Nernst–Einstein equation (see *e.g.* [24])

$$\sigma_{dc} = \frac{q^2 \mathcal{N} D}{k_B T} . \tag{3}$$

Here, q is the ion charge, $\mathcal{N}$ is the number density of mobile ions, k_B is the Boltzmann constant and T the temperature.

The numerical results for the dc conductivity *vs.* insulator volume content p are shown in Fig. 8 for various grain sizes a and enhancement factors τ. In all model calculations, we assumed a fixed interface thickness $\lambda = 1\,\text{nm}$. The figure shows that this microscopic model, which treats nano- and microcrystalline samples in exactly the same way (the only difference is the size of the grains) is able to reproduce all qualitative features of the experimental results (*cf*. Fig. 2). One feature cannot be reproduced by the model, however, namely the very high insulator concentration where the conductivity drops to zero. We will come back to this point at the end of the next section.
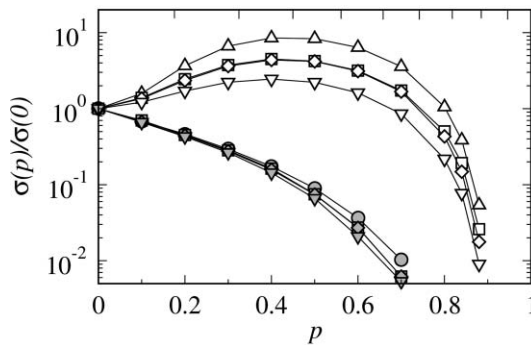
Fig. 8. Numerical results of the normalized dc conductivity $\sigma(p)/\sigma(0)$ *vs.* insulator volume fraction p in the brick-layer type percolation model for different grain sizes a and enhancement factors $\tau = \sigma_A/\sigma_B$. In all cases the interface thickness $\lambda = 1$ nm is fixed. Nanocrystalline grains: $\triangle$ $a = 10$ nm, $\tau = 200$; $\square$ $a = 10$ nm, $\tau = 100$; $\diamond$ $a = 20$ nm, $\tau = 200$; $\triangledown$ $a = 20$ nm, $\tau = 100$; Microcrystalline grains: $\bullet$ $a = 10\,\mu$m, $\tau = 200$; $\blacksquare$ $a = 10\,\mu$m, $\tau = 100$; $\blacklozenge$ $a = 20\,\mu$m, $\tau = 200$; $\blacktriangledown$ $a = 20\,\mu$m, $\tau = 100$ [20].
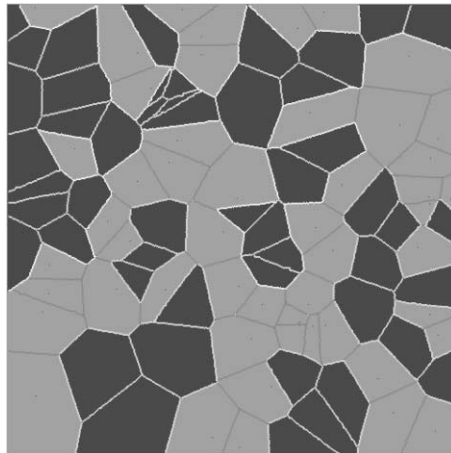

Fig. 9. Polycrystalline composite material created by Voronoi construction in two dimensions. Dark grey areas represent the ionic conductor grains and light grey areas represent the insulator grains.

4.3 Voronoi construction

To get a more realistic structure of the composites in our model description (compared to the over-simplified cubic arrangement) we used a Voronoi approach [25], see Fig. 9 for a two-dimensional sketch. 2000 seeds which represent the centers of the grains have been placed randomly inside a volume of 150^3 lattice sites. The borders of the grains are defined by the planes perpen-
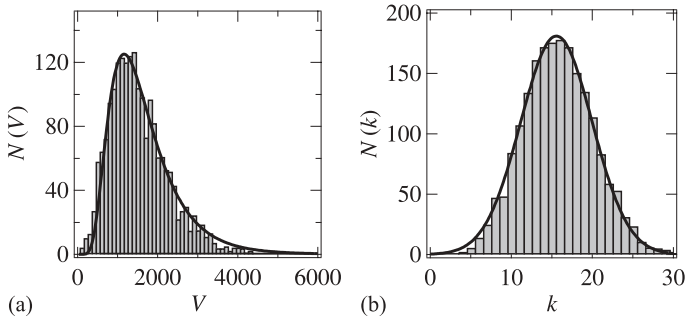
Fig. 10. The distribution of (a) grain volumes and (b) coordination numbers found for a Voronoi system on a lattice of 150^3 lattice sites with 2000 Voronoi cells. The volumes are given in units of the volume of an elementary lattice cell. The solid lines represent fits with a log-normal distribution of grain volumes (Eq. (4)) and a normal distribution of coordination numbers (Eq. (5)), respectively.

dicular to the connection line between two neighboured seeds intersecting this line exactly in the middle between both seeds. By this a fully compacted structure of irregular polyhedra is created. The shapes of the individual grains differ significantly and thus the number of edges of a crystallite does also change which results in a locally varying coordination number. Furthermore the particles are not mono-disperse but show a distribution of grain sizes.

Figs. 10(a) and (b) show the distributions of grain volumes and local coordination numbers, respectively, of the Voronoi system. The distributions can be fitted by a log-normal distribution of grain volumes

$$g(V) = \frac{N_0}{\sqrt{2\pi}V\sigma_V} \exp\left(-\frac{(\ln V - \ln V_0)^2}{2\sigma_V^2}\right) \tag{4}$$

and a normal distribution of coordination numbers

$$f(k) = \frac{N_0}{\sqrt{2\pi}\sigma_k} \exp\left(-\frac{(k - k_0)^2}{2\sigma_k^2}\right) , \tag{5}$$

respectively. The volumes are given in units of the volume of an elementary lattice cell. The overall number of cells, N_0, is equal to the number of seeds, and the fit yields $V_0 = 1474$ and $\sigma_V = 0.49$. The average coordination number was found to be $k_0 = 15.6$ and the standard deviation was $\sigma_k = 4.41$.

The structure created by the Voronoi construction (see Fig. 9) seems to represent quite nicely a real polycrystalline material (though pores are not included). The cells in Fig. 9 can now be regarded as insulating with probability p and as ionically conducting with probability $(1 - p)$, irrespective of their size.

It is clear that the dc conductivity will show a similar behavior as in the two models before. The main question that arises is whether the more realistic Voronoi construction is able to describe the conductivity close to $p = 1$
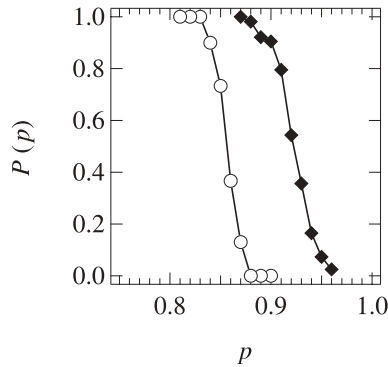
Fig. 11. The percolation probability $P(p)$ of the ionically conducting particles *vs.* insulator volume fraction p in the three-dimensional Voronoi system shown as white spheres. The black squares represent the case where Li ions can pass along B_2O_3/B_2O_3 interfaces being shorter than the average grain diameter.

in a better manner than the previous models. To this end, we determined the percolation probability $P(p)$ for ionically conducting particles to percolate the system. The result is shown in Fig. 11. One can see that the critical concentration p_c above which the conducting paths get disrupted is close to ≈ 0.86, being even smaller than the value we obtained for the brick-layer model in the foregoing section.

A reason for this underestimation of p_c might be that Li ion transport is also possible in the interface between insulating nanocrystalline grains, representing an additional Li diffusion passageway of nanometer length. Indeed, the percolation threshold increases to about 0.93 (see Fig. 11) if B_2O_3/B_2O_3 interfaces are considered to be permeable for Li ions (thus linking two non-directly connected Li_2O grains) if the length of these interfaces is smaller than the average particle diameter. In the brick-layer model, the assumption of such a 'nanometer-passageway diffusion' yields a threshold close to 0.95 [20].

5. Discussion

Summarizing the experimental results of the micro- and nanocrystalline composites we can conclude that they behave different in the following points: *(i)* The dc and ac conductivities of the microcrystalline samples decrease monotonically with insulator content x whereas they go through a maximum for the nanocrystalline samples. *(ii)* The dc and ac activation energies of the nanocrystalline samples show essentially no dependence on the insulator content x whereas they increase and decrease, respectively, with increasing x for the microcrystalline materials. *(iii)* The conductivity exponent n increases with
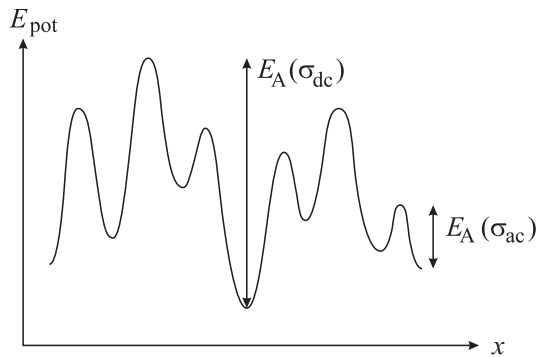
Fig. 12. Potential landscape for the movement of the Li ions. The ac conductivity probes dynamics on shorter length scales and thus gives lower activation energies than the dc conductivity.

x for the microcrystalline samples whereas it decreases for the nanocrystalline samples.

The fact that the activation energies of the nanocrystalline samples show no dependence on the insulator content x (Fig. 3) proves that the maximum in the dc and ac conductivity (Fig. 2) is not caused by a reduced activation energy but by an enhanced concentration of charge carriers. The fact that the activation energies for the ac conductivity are smaller than those for the dc conductivity in all cases suggests that the Li ions are moving in a potential landscape similar to that sketched in Fig. 12. The ac conductivity represents the short-range movement of the Li ions and therefore they have to overcome only the local activation barriers. For the long-range movement which is probed by dc conductivity measurements the Li ions have to overcome larger barriers. In general, the potential landscape will be time dependent [14].

NMR measurements on the same samples have shown that in the nanocrystalline composites two species of Li ions can be discriminated which have different mobilities whereas in the microcrystalline composites only the slower species is present [26, 27]. It can be concluded that in the nanocrystalline composites the Li ions with the higher mobility are located in the interfaces between the crystallites whose volume fraction is negligible in the microcrystalline composites. This has been corroborated in a further NMR study on the analogous composite system $(1 - x)$Li$_2$O : xAl$_2$O$_3$ [28].

6. Conclusion

Ac and dc conductivity measurements are able to show up the differences in short-range and long-range ionic motion in nano- and microcrystalline composites of a Li ion conductor and an insulator. Different theoretical approaches

have been presented which are suited to reproduce the dependence of the dc conductivity on *(i)* the composition and *(ii)* the grain size as well as the percolation thresholds. Both the continuum percolation model and the brick-layer type bond percolation approach yield the conductivity enhancement for the nanocrystalline composites and the monotonic decrease for the microcrystalline samples. Essential is an enhanced conductivity at the interfaces between the two components. The modelling of polycrystalline material by a Voronoi construction leads to the right distribution of grain sizes and a reasonable average coordination number. Assuming that the Li ions in the nanocrystalline composites are able to move not only in the Li_2O grains and in the interfaces between hetero-phases but also in B_2O_3/B_2O_3 interfaces if these are shorter than the average grain diameter, the correct percolation threshold for the disruption of the very last conducting pathways is obtained.

Acknowledgement

References

1. H. Gleiter, Progr. Mater. Sci. **33** (1989) 223.
2. R. W. Siegel, in *Encyclopedia of Applied Physics*, G. L. Trigg, E. H. Immergut, E. S. Vera, W. Greulich, Eds., VCH, New York (1994), p. 173.
3. H. Gleiter, Acta Mater. **48** (2000) 1.
4. H. Gleiter, Phys. Stat. Sol. (b) **172** (1992) 41.
5. P. Heitjans and S. Indris, J. Phys.: Condens. Matter **15** (2003) R1257.
6. P. Heitjans, A. Schirmer, and S. Indris, in *Diffusion in Condensed Matter – Methods, Materials, Models*, P. Heitjans, J. Kärger, Eds., Springer, Berlin (2005), in press.
7. J. Maier, Solid State Ion. **154**–**155** (2002) 291.
8. J. Maier, Solid State Ion. **157** (2003) 327.
9. J. Maier, Z. Phys. Chem. **217** (2003) 415.
10. J. Maier, *Physical Chemistry of Materials: Ions and Electrons in Solids*, Wiley, Chichester (2004).
11. S. Indris, P. Heitjans, H. E. Roman, and A. Bunde, Phys. Rev. Lett. **84** (2000) 2889.
12. S. Indris and P. Heitjans, Mater. Sci. Forum **343**–**346** (2000) 417.
13. S. Indris, D. Bork, and P. Heitjans, J. Mater. Synth. Process. **8** (2000) 245.
14. K. Funke, Prog. Solid. St. Chem. **22** (1993) 111.
15. K. Funke, C. Cramer, and B. Roling, Glastech. Ber. Glass Sci. Technol. **73** (2000) 224.
16. K. Funke and R. D. Banhatti, Solid State Ion. **169** (2004) 1.
17. K. Funke, C. Cramer, and D. Wilmer, in *Diffusion in Condensed Matter – Methods, Materials, Models*, P. Heitjans, J. Kärger, Eds., Springer, Berlin (2005), in press.
18. A. Bunde, W. Dieterich, P. Maass, and M. Meyer, in *Diffusion in Condensed Matter – Methods, Materials, Models*, P. Heitjans, J. Kärger, Eds., Springer, Berlin (2005), in press.
19. W. Dieterich and P. Maass, Chem. Phys. **284** (2002) 439.

20. M. Ulrich, A. Bunde, S. Indris, and P. Heitjans, Phys. Chem. Chem. Phys. **6** (2004) 3680.
21. A. Bunde and S. Havlin, Eds., *Fractals in Disordered Systems*, Springer, Berlin (1996).
22. A. G. Rojo and H. E. Roman, Phys. Rev. B **37** (1988) 3696.
23. H. E. Roman, J. Phys.: Condens. Matter **2** (1990) 3909.
24. A. R. Allnatt and A. B. Lidiard, *Atomic Transport in Solids*, Cambridge University Press, Cambridge (2003).
25. A. Okabe, B. Boots, and K. Sugihara, *Spatial Tessellations: Concepts and Applications of Voronoi Diagrams*, Wiley, Chichester (1992).
26. S. Indris, P. Heitjans, H. E. Roman, and A. Bunde, Defect and Diffusion Forum **194**–**199** (2001) 935.
27. S. Indris and P. Heitjans, J. Non-Cryst. Solids **307**–**310** (2002) 555.
28. M. Wilkening, S. Indris, and P. Heitjans, Phys. Chem. Chem. Phys. **5** (2003) 2225.